Direct structural determination in ultrathin ferroelectric films by analysis of synchrotron x-ray scattering measurements

D. D. Fong,[1,*] C. Cionca,[2] Y. Yacoby,[3] G. B. Stephenson,[1] J. A. Eastman,[1] P. H. Fuoss,[1] S. K. Streiffer,[1]
Carol Thompson,[4] R. Clarke,[5] R. Pindak,[6] and E. A. Stern[7]
[1]*Materials Science Division, Argonne National Laboratory, Argonne, Illinois 60439, USA*
[2]*Department of Physics, University of Michigan, Ann Arbor, Michigan 48109-1120, USA*
[3]*Racah Institute of Physics, Hebrew University, Jerusalem 91904, Israel*
[4]*Department of Physics, Northern Illinois University, DeKalb, Illinois 60115, USA*
[5]*FOCUS Center, Department of Physics, University of Michigan, Ann Arbor, Michigan 48109-1120, USA*
[6]*National Synchrotron Light Source, Brookhaven National Laboratory, Upton, New York 11973, USA*
[7]*Physics Department, University of Washington, Seattle, Washington 98195-1560, USA*
(Received 15 September 2004; published 27 April 2005)

In order to better understand ferroelectricity in thin films, it is important to explore the atomic-scale structure and the spatial distribution of polarization near the interfaces. We present sub-Ångstrom-resolution electron density maps of three ultrathin $PbTiO_3$ films grown epitaxially on $SrTiO_3$ (001) substrates. The maps were obtained by analysis of synchrotron x-ray scattering measurements of Bragg rod intensities using the recently developed coherent Bragg rod analysis method. A four- and a nine-unit-cell-thick film were studied at room temperature, and a nine-unit-cell-thick film was studied at 181 °C. The results show that at room temperature, the $PbTiO_3$ films are polar, monodomain, and have their polarization oriented away from the substrate. The four-unit-cell film may be the thinnest monodomain perovskite film found to be in the polar phase. At 181 °C, the electron density map of the nine-unit-cell film is consistent with the presence of 180° stripe domains. In the monodomain samples, details of the atomic-scale structure of the $PbTiO_3/SrTiO_3$ interface are observed, which may provide evidence for the nature of the positive charge layer required to stabilize polarization in monodomain films.

DOI: 10.1103/PhysRevB.71.144112 PACS number(s): 77.84.−s, 61.10.Eq, 68.35.−p, 77.22.Ej

I. INTRODUCTION

The exceptional materials properties exhibited by ferroelectric perovskites are being exploited in a variety of thin film applications, such as nonvolatile memories that rely on ferroelectric properties[1] and microelectromechanical systems and sensors that utilize their piezoelectric or pyroelectric properties.[2] As devices have become smaller and ferroelectric films thinner, the materials properties of thin films often deviate from their bulk counterparts, which can be attributed to the growing influence of interfacial effects.[3,4] From general theoretical considerations, changes in the ferroelectric order parameter, polarization, are expected near interfaces.[5] In addition, the extent to which the depolarizing field is screened, by excess charge at the interface and/or by domain formation, is crucial to determining the stability of the polar state in ultrathin films. The mechanisms by which screening occurs, and the extent to which polarization and the corresponding atomic structure vary in the proximity of ferroelectric interfaces, are among the most important unresolved questions in the physics of ferroelectrics.

Current understanding of paraelectric-ferroelectric and ferroelectric-ferroelectric interfaces is based primarily on theory. For films polarized perpendicular to the surface, as required by most devices,[6] an effective-Hamiltonian calculation found an enhancement of polarization near the surface in ultrathin $PbTiO_3$ films,[7] although a more recent *ab initio* study found that the enhancement could become a suppression depending on the direction of polarization.[8] In the above work, an ideal external field was supplied to stabilize the polar phase by cancelling the depolarizing field arising from the divergence of the polarization at the film interfaces. Understanding the degree of depolarizing field cancellation is important because the remaining field affects the polarization of the entire film. According to continuum theory[9–11] even metallic electrodes are unable to provide sufficient free charge density to fully screen the depolarizing field in ultrathin ferroelectric films. This concurs with *ab initio* calculations showing that imperfect screening by electrodes can produce a minimum thickness for ferroelectricity in monodomain films.[12] When sufficient free charge is not available, the alternative mechanism for reducing the energy of the depolarizing field is the formation of 180° stripe domains, consisting of an in-plane periodic lamellar structure in which the polarization alternates in sign.[13] Equilibrium 180° stripe domains have a period which is proportional to the square root of film thickness, owing to a trade-off between domain wall and electric field energy. The presence of such stripe domains in thin films with no electrodes has been predicted in phenomenological[14] and shell-model[15] calculations.

Recent experimental results have confirmed some aspects of this theoretical picture and raised questions about others. Formation of equilibrium 180° stripe domains has indeed been observed in epitaxial $PbTiO_3$ films on $SrTiO_3$ substrates.[16,17] The stripes produce satellite peaks in the diffuse x-ray scattering around $PbTiO_3$ Bragg peaks. Although in this system the stripe domain satellites always form when the sample is cooled from the nonpolar phase into the polar

phase, the satellites often disappear at lower temperature when samples are cooled sufficiently slowly,[16] suggesting that the sample becomes monodomain. This indicates that screening of depolarizing field by interfacial charge can occur even when no electrode is present (i.e., the substrate is insulating), and that monodomain ferroelectricity can be stable in $PbTiO_3$ films only a few unit cells thick. The nature of the charge at the interface with the insulating $SrTiO_3$ is not understood. These results emphasize the need for definitive experimental determination of the variation of polarization and atomic structure at ferroelectric interfaces.

Measurements of interfacial structure in ultrathin ferroelectric films have not been made previously due to the difficulty in growing ultrathin films with the requisite crystal quality, as well as the lack of a technique providing sufficient resolution that does not disturb the polarization. In this paper we present sub-Ångstrom-resolution maps of the atomic positions in three ultrathin $PbTiO_3$ films grown epitaxially on $SrTiO_3$ (001) substrates. The electron density maps were obtained using a recently developed x-ray method called coherent Bragg rod analysis (COBRA).[18,19] In this method, applicable to epitaxial thin films, we calculate complex scattering factors (CSFs) from measured x-ray scattering intensities along substrate-defined Bragg rods and obtain the three-dimensional structure by Fourier transforming the CSFs into real space. Phase information for the CSFs is obtained using an *ansatz* unique to the COBRA method, coupled with an iterative procedure related to those used in other direct methods for surface structure determination[20] and in coherent diffraction x-ray microscopy.[21] The COBRA ansatz allows the structure to be obtained with relatively few iterations.

Several features of the $PbTiO_3/SrTiO_3$ system make it particularly attractive for a COBRA study. A prototypical perovskite-structure ferroelectric, $PbTiO_3$ exhibits large spontaneous polarization and correspondingly large atomic displacements. Furthermore, the compressive epitaxial strain due to lattice matching of $PbTiO_3$ to $SrTiO_3$ causes polarization to occur preferentially along the surface normal,[22] which maximizes depolarizing field effects. Finally, as an end member of the widely used $Pb(Zr_xTi_{1-x})O_3$ system, $PbTiO_3$ thin films have been the subject of many theoretical and experimental investigations.[7,8,16,17,22–27] Extensive studies have been performed using *in situ* synchrotron radiation scattering to characterize the epitaxial growth of $PbTiO_3$ on $SrTiO_3$ (001) by metalorganic chemical vapor deposition (MOCVD),[28] the $PbTiO_3$ surface structure,[27] and the dependence of the ferroelectric phase transition on strain and film thickness.[16,17] A study of epitaxial films in which the x-ray scattering in the Bragg rods was fit to various models[24] showed that one can determine whether the film is monodomain and also the orientation of the polarization in a monodomain film from the interference between the scattering from the substrate and the film. In that study, it was found that the scattering from a 100 Å thick sample at room temperature was consistent with a simple model—a film of uniform polarization having the bulk value, with the polarization pointing down (into the substrate). For reference, we present a schematic of the $PbTiO_3$ unit cell in Fig. 1(a) and a depiction of coherently strained $PbTiO_3$ films with up and down polarizations in Fig. 1(b).

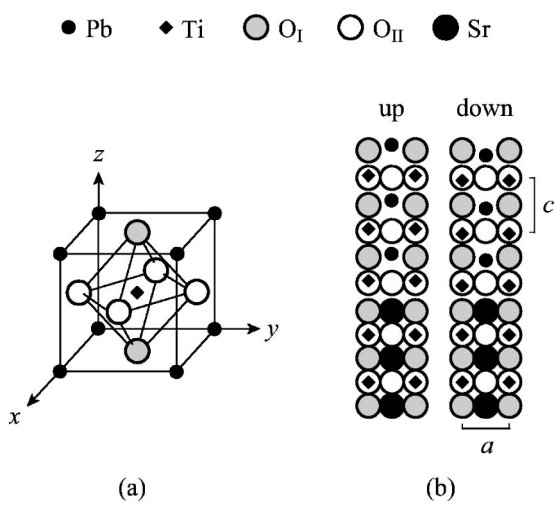

FIG. 1. Diagrams of the $PbTiO_3$ structure. (a) $PbTiO_3$ unit cell with atoms in their centrosymmetric positions. (b) Coherently strained $PbTiO_3$ films on $SrTiO_3$ (001) substrates with atoms projected onto (100) demonstrating up and down polarizations. In-plane and out-of-plane lattice parameters, *a* and *c*, respectively, are shown, here defined using the O_{II} positions.

Several questions helped motivate the current study. Not only are we interested in the domain structure and orientation in ultrathin films at room temperature, but we would also like to determine the polarization distribution throughout the film thickness. Our approach is to obtain high-resolution electron density maps using COBRA to provide this detailed information, namely the positions of all atoms within a column of unit cells spanning across the film thickness. In addition, study of a film at higher temperature which contains 180° stripe domains allows us to explore COBRA analysis of a sample with coherently diffracting domains.

The paper is organized as follows. In Sec. II, we describe the sample preparation. The Bragg rod measurements and results are discussed in Sec. III. In Sec. IV, we briefly explain the principles of the COBRA method and the specific steps followed in the present investigation. The structural results are presented and discussed in Secs. V and VI, and the paper concludes with a summary in Sec. VII.

II. SAMPLE PREPARATION

All of the samples were grown using a vertical-flow MOCVD growth chamber mounted on a horizontal-diffraction-plane *z*-axis goniometer located at the BESSRC beamline at sector 12 of the Advanced Photon Source (APS).[29] The $PbTiO_3$ films were grown epitaxially on $SrTiO_3$ (001) substrates as described previously.[28] The typical substrate miscut angle was 0.2°. Prior to growth, the $SrTiO_3$ substrates were etched in buffered HF to produce a surface with single-unit-cell high steps and TiO_2 layer termination.[30] For $PbTiO_3$ film growth, tetraethyl lead and either titanium isopropoxide (samples 1 and 2) or titanium tertbutoxide (sample 3) were used as the cation precursors, O_2 was the oxidant, and N_2 was the carrier gas. The total system pressure was 10 Torr (P_{O_2}=2.5 Torr), and growth was carried out

at 700 °C. Suitable PbO vapor over-pressure to maintain stoichiometry[28] was supplied while the sample was at high temperature. The $PbTiO_3$ films remained coherently strained to the substrates and replicated their high crystalline quality (0.01° typical mosaic). Real-time x-ray monitoring of the Bragg rod intensity during growth allowed control of film thickness to single-unit-cell accuracy.

Three samples were grown and studied. Samples 1, 2, and 3 had nominal thicknesses of 4, 9, and 9 unit cells, respectively. In order to obtain films without 180° stripe domains, samples 1 and 2 were both cooled slowly to room temperature, over a period of 24 hours. They were then taken out of the growth chamber for *ex situ* measurements. Sample 3 was cooled to 181 °C in roughly 5 hours to produce a 180° stripe domain structure. It was studied *in situ* in the growth chamber.

III. BRAGG ROD INTENSITY MEASUREMENTS AND RESULTS

The room temperature x-ray studies of samples 1 and 2 were performed at the MHATT beamline at sector 7 and the PNC beamline at sector 20 of the APS. The experimental setup has been described in Ref. 18. Measurements were made at an x-ray energy of 10 keV on Bragg rods with H and K from 0 to 3, over an L range that varied from rod to rod (typically 0.5 to 3.1), where H, K, and L are Miller indices given in the reciprocal lattice units of cubic $SrTiO_3$ (lattice parameter 3.905 Å). Nine of the 10 symmetry-independent Bragg rods within this range were measured, the exception being the 33L.

Sample 3 was studied at 181 °C in the MOCVD chamber at APS sector 12 described above. A moderately high energy (24 keV) was used to penetrate the 2-mm-thick quartz walls of the chamber, and a grazing-incidence geometry was used at fixed incidence angle of 1 degree.[31] For this sample only three Bragg rods were measured, 22L, 30L, and 31L. These rods were along azimuths that allowed the splitting of the Bragg rods caused by substrate miscut to be integrated by the resolution function. The higher x-ray energy and geometry of the chamber walls allowed L to be sampled from 0.2 to 4.2. At every L value, a K scan was performed and the background under the peak was subtracted.

Since it is conceivable that absorption of x rays could affect the polarization behavior of the film, studies were carried out to search for signs of x-ray interaction with sample structure. The $PbTiO_3$ films were subjected to various doses of 24 keV x rays with no discernible effect on the x-ray diffraction intensities.

All the intensities shown and used in the analysis have been corrected for optical polarization and geometrical factors.[32] A typical example of the intensity along a Bragg rod for each of the samples is shown in Fig. 2.

IV. COHERENT BRAGG ROD ANALYSIS (COBRA)

The COBRA method has been discussed in detail in Ref. 18. The goal is to obtain the unknown phases of the complex structure factors (CSFs) corresponding to the measured scattering intensities along the Bragg rods, in order to be able to determine the electron density distribution using a Fourier transform. An iterative procedure is used, as shown in Fig. 3. We begin with an initial reference structure, which is an approximate model of the structure of the sample, including the substrate. The total electron density (ED) of the sample can be decomposed into the sum of the ED of the reference structure and an unknown difference ED. Similarly, the total CSFs of the sample are sums of CSFs from the reference

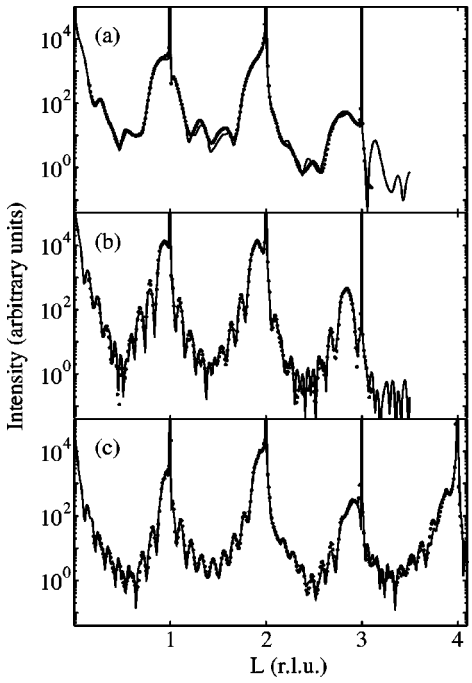

FIG. 2. Comparison of measured intensities (points) and COBRA-calculated intensities (solid curves) along representative Bragg rods for each sample, (a) 00L of sample 1, (b) 00L of sample 2, (c) 22L of sample 3. The total number of rods used in the COBRA analysis was 9, 9, and 3 for samples 1, 2, and 3, respectively.

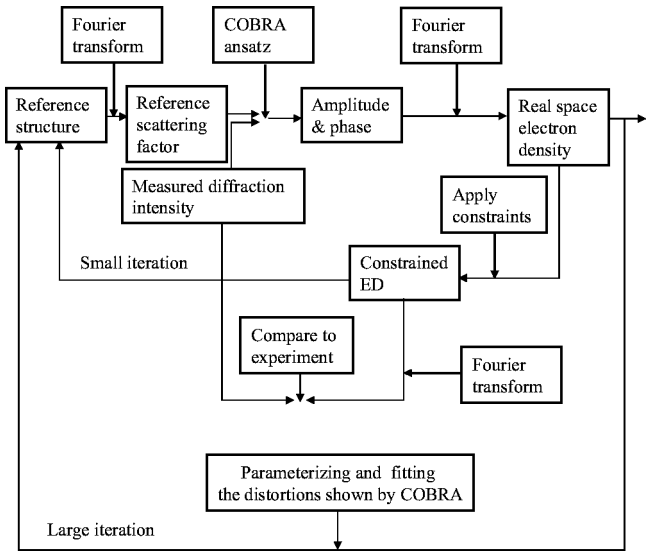

FIG. 3. Flow diagram of the COBRA data analysis procedure.

structure and the unknown difference. Using the experimentally measured intensities and the calculated reference CSFs, an *ansatz* is used to obtain the unknown difference CSFs. The *ansatz* is based on the assumption that the unknown CSF varies more slowly along the Bragg rod than the reference CSF. The error associated with this assumption is diminished by taking advantage of the fact that the known part of the sample and the unknown part are spatially separate, and the error decreases with each iteration as the unknown CSFs become progressively smaller.[18,19] The total CSFs are then Fourier transformed into real space, yielding a trial solution for the three-dimensional real space ED of the sample. (A Gaussian window function is applied prior to Fourier transforming to reduce truncation artifacts.) To be an acceptable ED, this function must be positive everywhere, zero outside the sample, and approach the known structure deep within the substrate. In general, however, the trial solution obtained will be in violation of these requirements, and so these constraints are imposed on the solution. From the resulting ED function, we calculate scattered intensities and compare them with the measured intensities. If the agreement is unsatisfactory, the newly obtained ED is used to construct a new reference structure, and the whole procedure is iterated. Two methods are used to build the new reference structure. In the first method (the small iteration), we simply use the new ED as the reference structure. With the second method (the large iteration), we parametrize the distortions observed in the COBRA-obtained ED relative to the reference ED. These parameters are refined to obtain the best fit with the measured intensities using a standard least-squares-fitting procedure, and the resulting structure is used as the new reference structure.

For the present analysis, the initial reference structure used has all atoms in their centrosymmetric positions, with the film having the nominal number of unit cells and an out-of-plane lattice parameter chosen to give a rough agreement with the data. The electron density was constrained to the known $SrTiO_3$ structure at distances greater than 8 unit cells from the interface. We found that it was necessary to use both methods for building the new reference structure to obtain convergence, i.e., after each large iteration, two or three small iterations are performed. The nature of the displacements found in the small iterations give guidance on which parameters to choose (and their initial values) for performing the large iteration.

The COBRA method is generally applicable to systems that are periodic in two dimensions, aperiodic in the third, and commensurate with the underlying substrate, although it can also provide detailed structural information for systems that are only partially periodic in two dimensions and are nonuniformly strained or locally incommensurate with the substrate.[18] The result of the COBRA method is an electron density map of a single column of substrate-defined unit cells spanning across the film thickness. When the in-plane periodicity of the film is larger than that of the substrate, this ED represents the folded structure obtained by laterally translating all the atoms in the system into the column of substrate-defined unit cells using the substrate in-plane lattice vectors.[18]

Because of anomalous scattering corrections to the x-ray scattering factors, the electron density maps of the atomic cores reported here correspond in principle to the atomic scattering factors at $Q=0$, rather than to true electron densities. The true and effective numbers of electrons per atom[33] at 10 keV (for samples 1 and 2) and 24 keV (for sample 3) are given in Table I. The only significant difference is for Pb at 10 keV. Since it is difficult to measure scattering cross sections on an absolute scale to the same high accuracy possible with a relative intensity measurement, we have used an overall scale factor to normalize the electron densities obtained for each sample. This scale factor was chosen to give the correct integrated number of electrons per unit cell averaged over the deepest four displayed $SrTiO_3$ unit cells (i.e., 83.7 for samples 1 and 2 at 10 keV, and 84.3 for sample 3 at 24 keV).

TABLE I. Effective number of electrons per atom.

	Pb	Sr	Ti	O
True electron number	82	38	22	8
Scattering factor ($Q=0,10$ keV)	77.3	37.3	22.4	8.0
Scattering factor ($Q=0,24$ keV)	81.3	38.1	22.2	8.0

For samples 1 and 2, the intensity distribution was localized on the Bragg rod and no satellites appeared in the diffuse scattering [Fig. 4(a)], indicating that nanoscale 180° stripe domains were not present. These films are therefore either monodomain, or consist of large up and down domains where the associated diffuse scattering overlaps with the Bragg rod. In the latter case, the Bragg rod intensity will be the sum of the intensities from the up and down domains. The COBRA analysis cannot be applied to an incoherent sum of intensities, since it assumes a coherent sum of scattering amplitudes. In order to examine the possibility of a significant volume fraction of both up and down domains too large

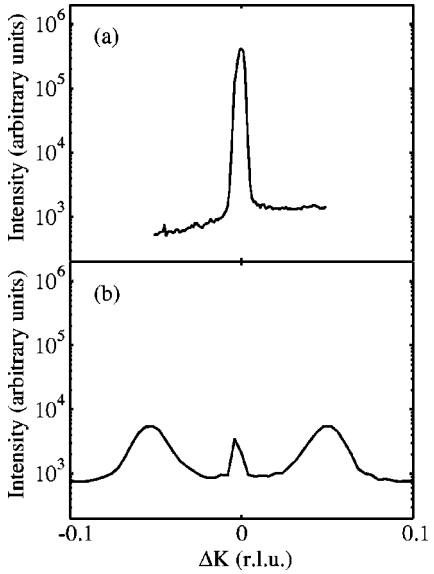

FIG. 4. In-plane scan through $PbTiO_3$ Bragg peaks showing absence or presence of satellites from nanoscale 180° stripe domains, (a) *K*-scan through 202 peak in sample 1, (b) *K*-scan through 304 peak in sample 3.

to resolve, the measured intensities were fit assuming that they were equal to the sum of intensities from oppositely polarized domains. Since we found that the best fit for such a procedure resulted in unrealistic values of the fitting parameters, we believe that samples 1 and 2 are monodomain. In this case the film is periodic in two dimensions with a period equal to that of the substrate. We therefore expect that the COBRA-calculated ED will be that of the actual structure. We have carried out the COBRA procedure for samples 1 and 2 and obtained convergence after one large iteration followed by two small iterations. Figures 2(a) and 2(b) show a comparison between the COBRA calculated and the measured intensities along the 00*L* Bragg rod for samples 1 and 2, respectively. The excellent agreement between the two is typical for all the other Bragg rods and supports our assumption that these samples are in a single domain state.

The analysis of sample 3 differed in two respects. First, this film consists of 180° stripe domains periodically spaced along the in-plane ⟨100⟩-type directions and shows the associated satellites, as shown in Fig. 4(b). The satellites are well separated from the Bragg rod, and the background at the Bragg rod position due to this diffuse scattering from the domains was subtracted from the rod intensity prior to COBRA analysis. Thus the measured intensity on the rod arises from the coherent sum of the amplitudes from the domains, and the COBRA-calculated ED is expected to be that of the folded structure of the two types of domains. Second, for this sample the scattered intensities were measured only along three Bragg rods. This information can be sufficient to determine the full structure provided the system has no in-plane displacements except for simple thermal broadening. As discussed below, analysis of the data for samples 1 and 2 shows that there are no in-plane displacements, and we assume that this is also true for sample 3. In this case the CSF at any point *L* along a rod is a linear combination of the CSFs contributed by atoms along three lines in real space perpendicular to the surface, one going through the Pb and Sr atoms, the second through the Ti and O_I atoms, and the third going through the O_{II} atoms (see Fig. 1). For each *L*, there are three unknown atomic line CSFs and three measured intensities that are equal to the absolute value squared of the linear combination of the three atomic line CSFs. These equations cannot be solved directly for the line CSFs. However, using COBRA we can obtain the CSFs along each Bragg rod from the intensities measured along it. This results in three linear equations that can now be solved for the three atomic line CSFs. The line CSFs are then used to calculate the CSFs of all other Bragg rods, and we can continue with the COBRA procedure as before. For sample 3, we obtained convergence after two large iterations each followed by two or three small iterations. A comparison between the COBRA-calculated and measured intensity along the 22*L* Bragg rod [Fig. 2(c)] again shows excellent agreement and is typical of the other two Bragg rods.

V. FILM STRUCTURE: RESULTS AND DISCUSSION

Two-dimensional slices through the COBRA-calculated electron densities of samples 1, 2, and 3 are shown in Figs. 5, 6, and 7, respectively. Several duplicate columns of unit cells are shown for clarity. Two different planes normal to the surface are shown. In (a), we show a (110) plane cutting through the Sr, Pb, Ti, and O_I atoms, while in (b) we show a (100) plane through the Ti, O_I, and O_{II} atoms. All the atoms, including oxygen, are clearly visible as peaks in the electron density. The widths of the peaks are determined by the resolution of the x-ray data, which extend to only about four reciprocal lattice units, rather than the true atomic sizes.

Examination of the EDs on planes parallel to the surface showed no measurable in-plane atomic displacements in samples 1 and 2. We found no signature of the counter-rotated oxygen octahedra in the uppermost TiO_2 layer observed in the high-temperature surface reconstruction,[27] probably because it is difficult to discern such small in-plane displacements in the presence of surface roughness. In what follows, we focus solely on out-of-plane (*z*) displacements.

In Fig. 8 we present the electron density along three lines parallel to the surface normal. One line goes through the Pb and Sr atoms, the second goes through Ti and O_I atoms, and the third goes through the O_{II} atoms. The apparent negative electron density values, and the nonzero electron densities outside the sample, visible in Fig. 8 are an indication of the uncertainties in determination of the electron density. For samples 1 and 2, the negative parts are small and present only along the Sr/Pb line. The ED outside the film is also small. For sample 3, the negative parts of the ED are larger, as is the ED outside the film. We attribute this difference to the smaller dataset used for sample 3. Although three Bragg rods contain all the structural information, we believe that having nine Bragg rods leads to a better cancellation of systematic and stochastic errors. The contributions to the true ED of all Bragg rods add coherently, whereas the errors sum incoherently.

For all three samples, the atoms in the $SrTiO_3$ substrate far away from the interface (left-hand side of figures) all occupy their centrosymmetric positions. However, one can see evidence of polarization in the $PbTiO_3$ films. For samples 1 and 2, the Pb atoms in Figs. 5(a) and 6(a) are displaced relative to the Ti atoms in the outward direction, away from the $SrTiO_3$ substrate. Similarly, the Ti atoms in Figs. 5(b) and 6(b) are displaced relative to the O_{II} atoms in the same direction. In contrast, for sample 3, the Pb and Ti peaks in the film appear close to their centrosymmetric positions. However, the Pb electron density peaks are significantly broader in the *z* direction than the Sr peaks, and they have smaller peak intensities than the Pb peaks in samples 1 and 2. The Ti peaks also decrease in magnitude and broaden towards the surface. The broad, centered peaks suggest that the COBRA-derived electron density map consists of a folding of the oppositely polarized domains in a 180° stripe domain structure with nearly equal up and down cation displacements.

The electron densities in Figs. 5–7 were analyzed by fitting each atomic peak to a three-dimensional Gaussian function. The center of this fit gives the atomic position, and the integrated electron density gives the total number of electrons of the atom at that site. For sample 3, the Pb and Ti peaks were fit using the sum of two identical Gaussians equally displaced in *z* on each side of the center, as described below.

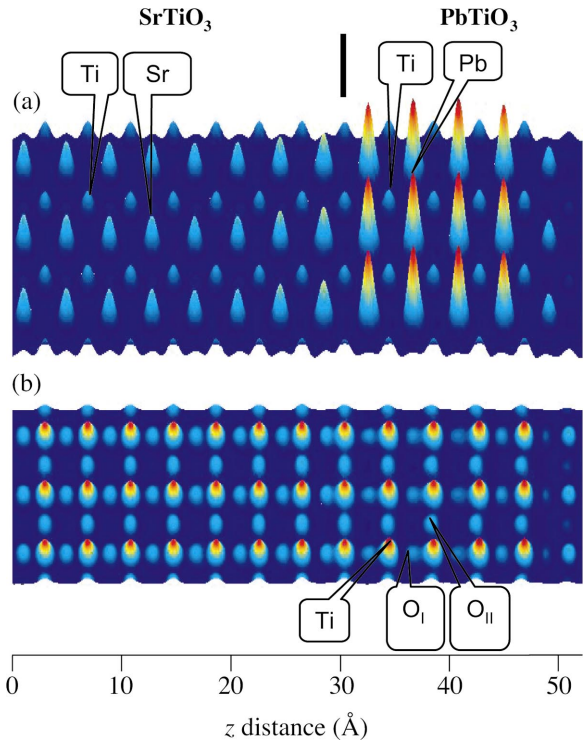

FIG. 5. (Color) The electron density of sample 1 with four $PbTiO_3$ unit cells at room temperature. (a) (110) plane through the Sr, Pb, Ti, and O_I atoms. (b) (100) plane through the Ti, O_I, and O_{II} atoms. Redder hues indicate higher intensities; intensity scale is expanded in (b) compared to (a).

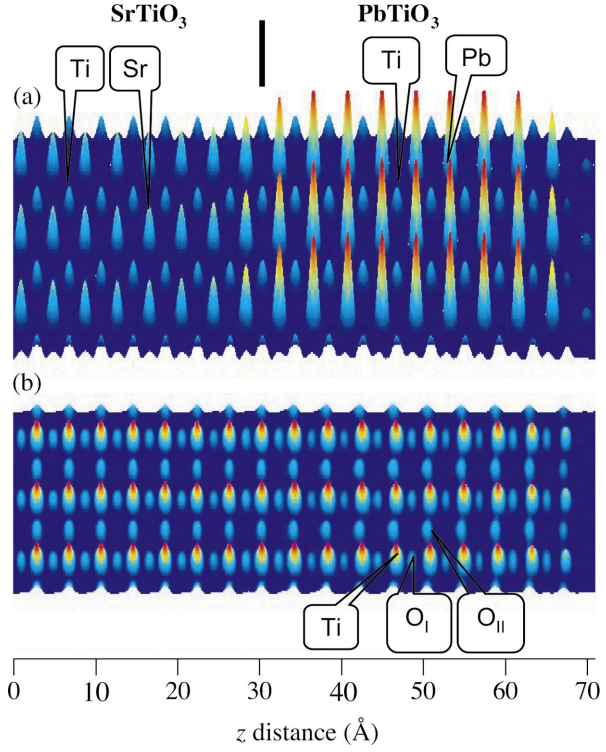

FIG. 6. (Color) The electron density of sample 2 with nine $PbTiO_3$ unit cells at room temperature, plotted as in Fig. 5.

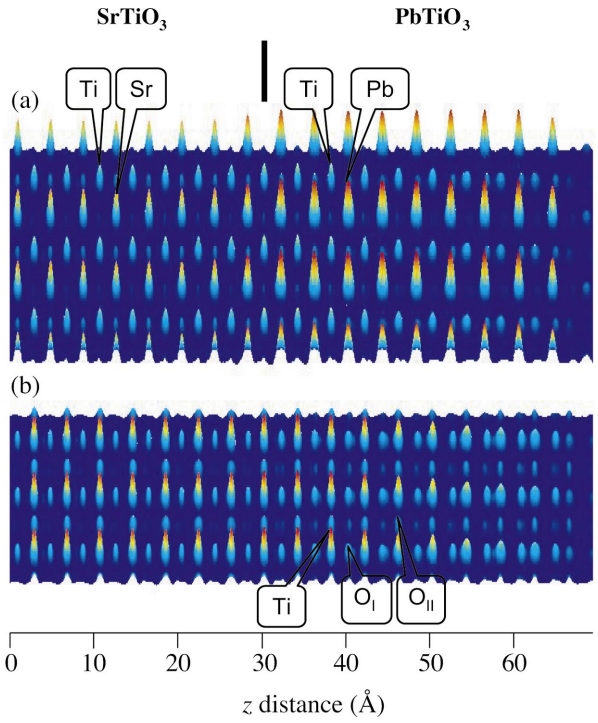

FIG. 7. (Color) The electron density of sample 3 with nine $PbTiO_3$ unit cells measured at 181 °C, plotted as in Fig. 5.

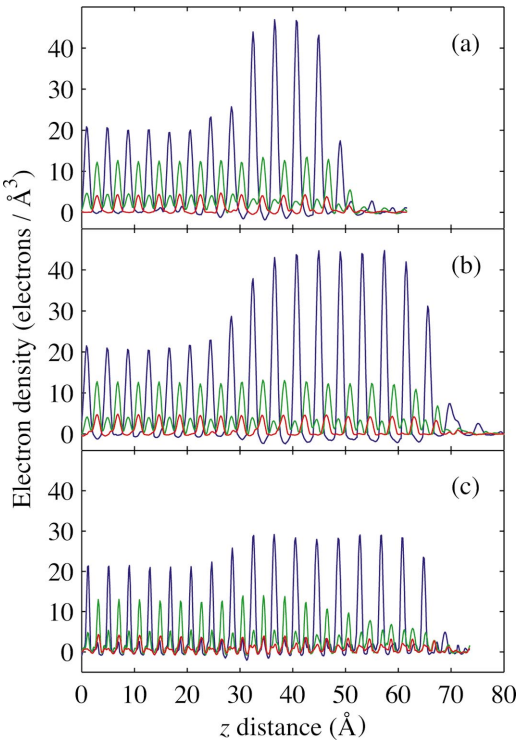

FIG. 8. (Color) Electron densities as function of z for samples 1 (a), 2 (b), and 3 (c). Blue lines are along the Sr/Pb atoms, green lines along Ti and O_I atoms, and red lines along the O_{II} atoms. The top-most eight unit cells of the $SrTiO_3$ substrate are on the left-hand side, and the surface of the $PbTiO_3$ film is on the right-hand side.

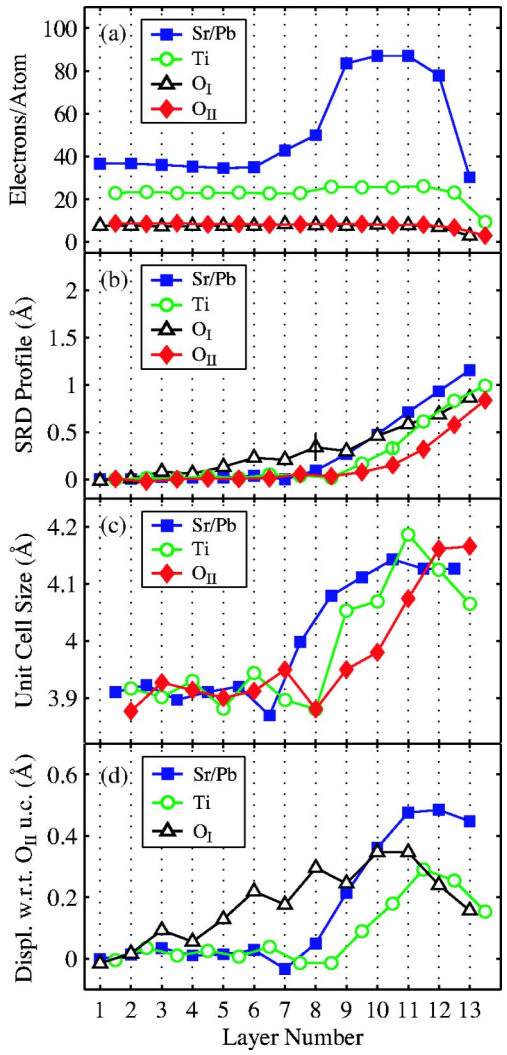

FIG. 9. (Color online) Summary of COBRA-determined electron numbers and atomic positions in sample 1.

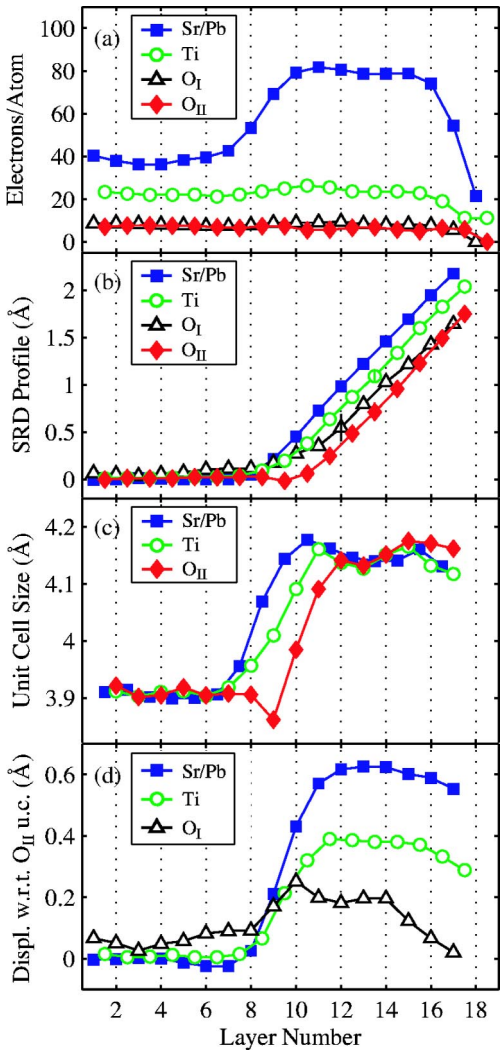

FIG. 10. (Color online) Summary of COBRA-determined electron numbers and atomic positions in sample 2.

A. Atomic positions, samples 1 and 2

Figures 9 and 10 summarize our results for samples 1 and 2, respectively. In graph (a), we show the number of electrons per atom for each of the four crystallographic sites, as a function of unit cell position in the sample. The layer number was chosen so that the Sr site at $z \approx 28$ Å corresponds to layer 8. The relative values for the different atoms agree quite well with the expected values given above. The number of electrons on the Sr/Pb site varies as expected between the substrate and film, while the numbers of electrons on the Ti and O sites remain relatively constant. The Sr/Pb curves indicate that the transition region between the substrate and film is approximately two unit cells thick in both samples. This could include contributions from both interface roughness and intermixing. At the surface, the transition region corresponds to a surface roughness of one to two unit cells in both samples. The Sr/Pb curves are consistent with $PbTiO_3$ film thicknesses of four and nine unit cells, respectively, for samples 1 and 2.

In order to display the atomic positions in an easily understood manner, in graph (b) we plot the out-of-plane displacements of the atoms relative to the corresponding positions in an ideal $SrTiO_3$ crystal, as if the substrate were extended into the region of the film, to obtain a "substrate relative displacement" (SRD) profile. To illustrate how to interpret the SRD profiles, calculated profiles from some idealized models are shown in Fig. 11, which depict films polarized up (a), (b) and down (c), (d). The first plane in the film to exhibit atomic displacements away from the centrosymmetric positions is either TiO_2 (a), (c) or PbO (b), (d). In these examples, we have assumed a nine-unit-cell-thick $PbTiO_3$ film of uniform polarization, with the fractional unit cell coordinates of the atoms given by the bulk values at room temperature shown in Table II, and the calculated epitaxially strained lattice parameter from Table III. The values in Table III are obtained from Landau-Ginzburg-Devonshire theory[22] for coherently strained $PbTiO_3$ on $SrTiO_3$. An additional parameter in these simple models is the spacing between the layers at the interface. Here we have chosen to keep the cation-defined lattice parameter equal to that on the film side.

The slope of the SRD profile for a given atomic site indicates the deviation of the unit cell size from the $SrTiO_3$ lat-

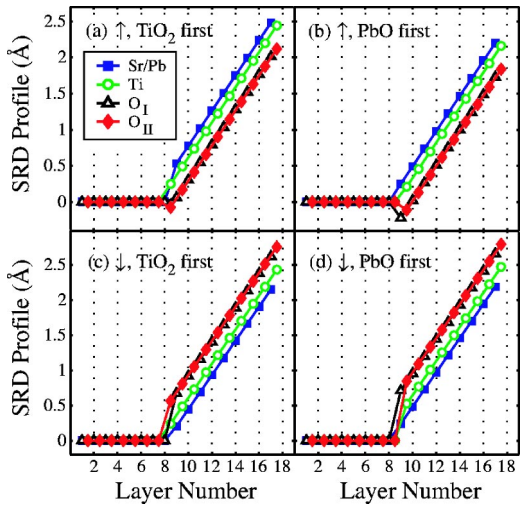

FIG. 11. (Color online) Calculated ideal SRD profiles for a film with up (a), (b) and down (c), (d) polarization, for each choice of first displaced layer.

tice parameter. In these idealized examples, the slopes of the SRD profiles for the various sites in the film are all constant and identical. In the actual data, the slopes vary with depth in the film, and differ depending upon which site is used to define the unit cell. The vertical distance between SRD profiles for different sites gives the relative atomic displacements referenced to centrosymmetric positions. In particular, it is easy to tell the polarization direction from the position of the SRD profiles of the cations relative to those of the anions. The nature of the displacements at the interface can also be discerned from the SRD profile.

The experimentally determined SRD plots are shown in Figs. 9(b) and 10(b). The unit cell sizes determined from the slopes of the SRD profiles are shown in graphs (c), and the Pb, Ti, and O_I displacements with respect to centrosymmetric positions in an O_{II}-defined unit cell are shown in graphs (d).

One can clearly see that the $PbTiO_3$ films in both samples are in the noncentrosymmetric (ferroelectric) phase, with a polarization oriented away from the surface (up)—that is, on average the cations are displaced away from the substrate relative to the anions. Based on the Pb sublattice, the average *c* lattice parameters of the four- and nine-unit-cell-thick films are 4.127 ± 0.013 Å and 4.150 ± 0.015 Å, respectively. The value for the nine-unit-cell-thick film agrees very well with that expected for an epitaxially strained film at 25 °C (Table III), indicating that the polarization in this ultrathin film is almost the same as in a thick film. The slightly smaller lattice parameter of the four-unit-cell-thick film is consistent with a slightly smaller polarization. This suggests that for both samples, significant free charge to screen the depolarizing field (~ 0.7 C/m^2 or ~ 0.7 electrons per unit cell area) must be present near the interfaces, positive at the substrate and negative at the surface. The four-unit-cell-thick film is one of the thinnest perovskite films yet demonstrated to be in the polar phase.[17] Interestingly, the average Pb and Ti displacements with respect to the O_{II} unit cell of the nine-unit-cell-thick film are larger than those expected for a thick epitaxial film (0.480 Å and 0.320 Å, respectively). The Pb-O_{II} and Ti-O_{II} displacements of the four-unit-cell-thick film are in better agreement with these values.

TABLE III. Landau-Ginzburg-Devonshire theory values for epitaxially strained $PbTiO_3$ on $SrTiO_3$ at zero field.

Temperature (°C)	25	181
c lattice parameter (Å)	4.149	4.130
Polarization (C/m^2)	0.745	0.694
Unit cell coordinate Δz_{Pb} (Å)	0.480	0.445
Unit cell coordinate Δz_{Ti} (Å)	0.320	0.297
Unit cell coordinate Δz_{O_I} (Å)	0.013	0.012
180° domain wall splitting S_{Pb} (Å)	0.673	0.623
180° domain wall splitting S_{Ti} (Å)	0.348	0.323
180° domain wall splitting S_{O_I} (Å)	0.301	0.280
180° domain wall splitting $S_{O_{II}}$ (Å)	0.186	0.172

Several details of the interface structure which were hitherto inaccessible can be observed in the data. In both samples, the Pb sublattice expands immediately to its maximum size as the interface is crossed, whereas the Ti and O_{II} sublattices expand one or two unit cells into the $PbTiO_3$ film, respectively. If the Ti and O_{II} atoms were to acquire their full displacement relative to Pb immediately at the interface, then the O_{II}-O_{II} and Ti-Ti distances across the interface would be compressed, relative to those in $SrTiO_3$. Apparently this is energetically unfavorable. The positions of the O_I atoms have a larger uncertainty than the other atoms. A typical error bar for the O_I positions (±0.14 Å) is shown in Figs. 9(b) and 10(b); the corresponding error bars for the other sites (±0.04 Å, ±0.05 Å, and ±0.10 Å, respectively, for Sr/Pb, Ti, and O_{II}) are smaller than the symbols. This larger uncertainty stems from the fitting of the O_I peak in the electron density, which is close to the Ti peak. Nevertheless, the O_I atoms show an unusual behavior near the interface in both samples. While the O_{II} displacements are zero or negative with respect to the cations throughout the heterostructure, consistent with the positive film polarization, the O_I displacements are posi-

TABLE II. Literature values for parameters.

Site	Pb/Sr	Ti	O_I	O_{II}	Reference
$PbTiO_3$ fractional coordinate $\Delta z/c$ (25 °C)	0.117	0.078	0.003	0.000	34
$PbTiO_3$ 180° domain wall splittings $S/\Delta z_{Pb}$ (0 K)	1.401	0.725	0.628	0.387	25
$PbTiO_3$ Born effective charges (0 K)	3.92	6.71	−5.51	−2.56	35
$SrTiO_3$ Born effective charges (0 K)	2.54	7.12	−5.66	−2.00	35

tive with respect to the cations near the interface and for several unit cells into the $SrTiO_3$. The O_I atoms are the only ones to show significant displacements on the $SrTiO_3$ side of the interface. This behavior of the O_I atoms at the interface will be discussed further below in the context of interfacial charges.

B. Atomic positions, sample 3

The in-plane 180° stripe domain structure of sample 3 makes interpretation of the electron density maps more challenging. We expect the COBRA-determined ED to be a superposition of the EDs from up and down domains in a given layer. This folding of the up and down domain structures, as well as the expected in-plane nonuniformities within the stripe domains due to electric field components at the interfaces, will tend to obscure fine details of the structure. To determine the splitting between the Pb-Pb and Ti-Ti positions in the up and down domains, we fit the Pb and Ti electron density peaks to a composite peak shape. Based on the behavior of samples 1 and 2, we assumed that the widths of the individual Pb and Ti atomic electron densities were the same as those of the Sr and Ti in the substrate, respectively. When the Pb (Ti) peaks were significantly broader than the single atom peaks in the substrate, they were fit to a sum of two Gaussians with equal magnitudes, with equal widths fixed to that of the substrate Sr (Ti) peak, with their z positions and magnitude allowed to vary.

Figure 12 summarizes our results for sample 3. The numbers of electrons per atom are shown in graph (a). For Pb and Ti in the film, these are the sum of the integrals of the two Gaussians. In the $SrTiO_3$ substrate, the relative values for the different sites agree with the expected values given above. However, the number of electrons for the Pb site in the film are generally lower than the expected value of 81.3. The values for the Pb and Ti sites decrease progressively towards the surface, while the O_{II} values increase. We believe that these deviations in total electron number are artifacts due to the errors in the experiments, the COBRA data analysis, and the fitting to two Gaussians. The interface thickness is approximately one unit cell.

The Pb and Ti positions shown in Figs. 12(b)–12(d) are the average of the up and down positions, while Fig. 12(e) shows the splitting between the Pb-Pb and Ti-Ti positions in the up and down domains for the positions where two Gaussians were fit. The electron densities around the oxygens are too small for a similar analysis to be meaningful. The average unit cell in sample 3 is 4.043 ± 0.005 Å. This is significantly smaller than the expected value of 4.130 Å from LGD theory for a monodomain film shown in Table III, consistent with a smaller average polarization in each domain. In Fig. 12(d), we see that within the uncertainties, the average atomic positions of the Pb and Ti atoms are nearly at the centrosymmetric positions relative to O_{II}. The slight positive displacement of the Pb curve may indicate the presence of more up than down domains. The average O_I positions deviate significantly in the upper part of the film.

The average splitting between the Pb atoms is 0.4 ± 0.1 Å. Additionally, in the top half of the film, the Ti atoms are also split by approximately 0.4 Å. The minimum discernible splitting is about 0.2 Å. This is in rough agreement with *ab initio* results for 180° domain walls in $PbTiO_3$ (Ref. 25) given in Table II, which shows offsets of the various sites at 0 K, normalized to the Pb displacement with respect to the O_{II} unit cell. In Table III these have been multiplied by the LGD theory results for the Pb displacement to give 0.623 and 0.323 Å, respectively, for the Pb and Ti splittings expected at

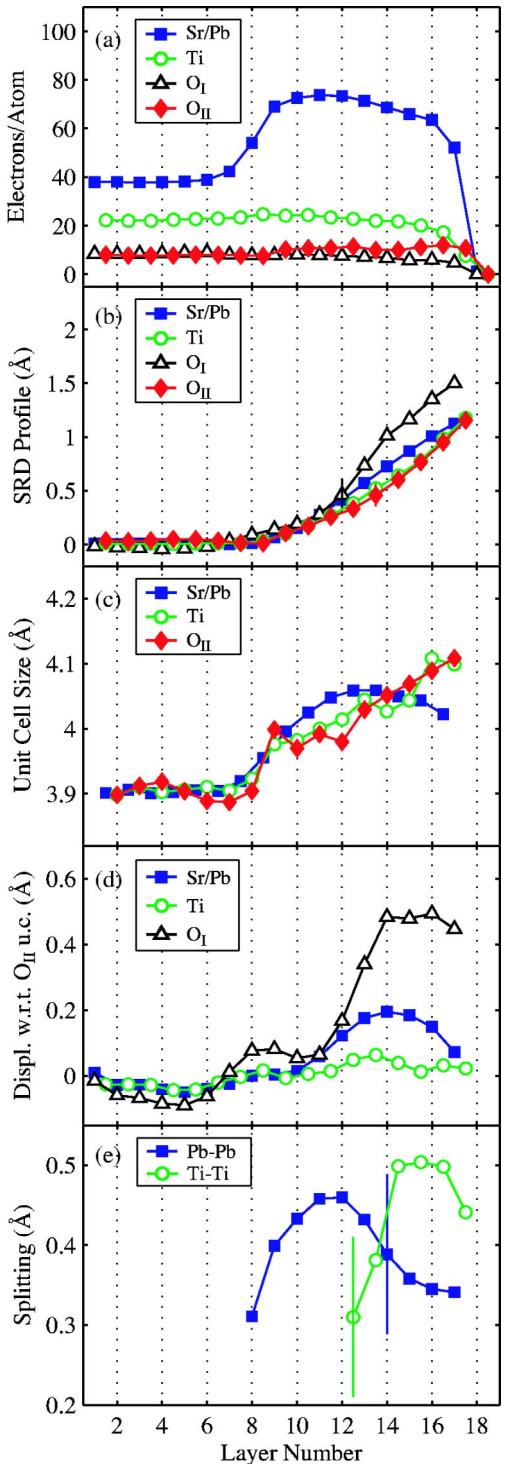

FIG. 12. (Color online) Summary of COBRA-determined electron numbers and atomic positions in sample 3.

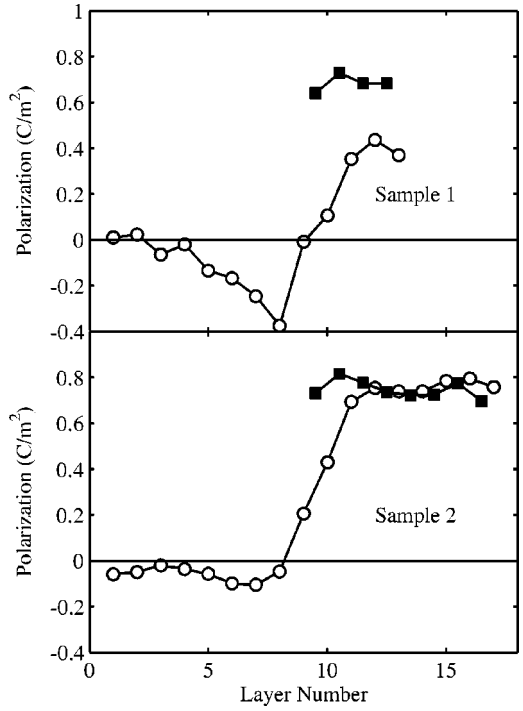

FIG. 13. Polarization distributions calculated using two methods. Solid squares, from $PbTiO_3$ film *c*-axis lattice parameter using LGD expression. Open circles, from Born effective charges for bulk materials. Both use unit cells with origin at Pb sites.

181 °C. This large splitting of the atomic peaks due to the 180° stripe domains causes the near cancellation of the $PbTiO_3$ 304 Bragg peak seen in Fig. 4(b).[31]

VI. INTERPRETATION AS A POLARIZATION DISTRIBUTION

It is interesting to interpret the atomic displacements determined by the COBRA analysis for the monodomain samples in terms of the polarization distributions in the films. Two methods can be used to relate the atomic positions to the polarization. According to LGD theory for coherently strained epitaxial films, the equilibrium polarization is related to the lattice parameter *c* by[22]

$$P = \left(\frac{x_3 - (2s_{12}/(s_{11}+s_{12}))x_m}{Q_{11} - (2s_{12}/(s_{11}+s_{12}))Q_{12}} \right)^{1/2}, \qquad (1)$$

where s_{ij} and Q_{ij} are material constants, and the out-of-plane and in-plane strains x_3 and x_m are defined from the respective lattice parameters *c* and *a* using the extrapolated lattice parameter *b* of the cubic paraelectric phase by $x_3=(c-b)/b$, $x_m=(a-b)/b$. Figure 13 shows the polarization distribution in samples 1 and 2 calculated with parameter values for epitaxially strained $PbTiO_3$ on $SrTiO_3$ using the *c* lattice parameter of the $PbTiO_3$ film obtained from the Pb-defined unit cells. Since the measured *c* lattice parameters are similar to that expected from LGD theory, the calculated polarizations are also similar (see Table III).

A second method to obtain polarization is by calculating the dipole moment per unit cell using the atomic positions Δz_i and the Born effective charges Z_i^* of each atom, using the relation

$$P = \sum Z_i^* \Delta z_i / \Omega_0, \qquad (2)$$

where Ω_0 is the unit cell volume, in our case a^2c. The Born effective charges for cubic $SrTiO_3$ and tetragonal $PbTiO_3$ calculated for bulk materials from *ab initio* theory[35] are given in Table II. Using these values and the measured atomic positions for bulk $PbTiO_3$ at room temperature given in Table II overestimates the polarization by a factor of 1.34. We have therefore divided the calculated Born effective charges in Table II by this factor. We used the measured atomic positions to calculate the polarization profiles for samples 1 and 2 shown in Fig. 13. These polarization profiles show an unexpected feature—the region of the $SrTiO_3$ substrate near the film is polarized in the opposite direction than the film. This would require that the polarization of the $PbTiO_3$ be overcompensated by free charge at the interface. It is more likely that the bulk values for Z_i^* are not valid near the interface. As seen in Figs. 9(b) and 10(b), it is the off-center O_I atoms in the $SrTiO_3$ that are producing the apparent negative polarization. These atoms have an unusually large negative Z^* in bulk $SrTiO_3$. If this were less negative near the interface it would give a more reasonable polarization profile and potentially explain the structural origin of the positive free charge needed for screening. Understanding of the nature of this charge compensation must occur before we can quantitatively compare atomic position measurements with theory. New *ab initio* calculations for ultrathin $PbTiO_3$ films on $SrTiO_3$ could shed light on the possible role of the O_I atoms in screening the depolarizing field.

At the film surface of the monodomain samples, we find no unusual O_I displacements, implying that a different mechanism of screening takes place at this interface. However, since the surface is exposed to ambient air, the nature of the chemical species present is not as well defined as it is at the substrate interface.

VII. SUMMARY AND CONCLUSIONS

We have described the x-ray measurements of three $PbTiO_3$ films grown epitaxially on $SrTiO_3$ (001) substrates and their structure as determined by the COBRA method. Samples of four- and nine-unit-cell thickness were cooled slowly to room temperature for *ex situ* measurements, while another nine-unit-cell-thick sample was measured *in situ* at 181 °C.

The room temperature results show that both samples are monodomain and polarized up, away from the substrate. Within the interface region, the Pb atoms are the first to assume the new unit cell dimension, while the Ti and oxygen atoms retain a smaller unit cell for one to two additional unit cells. This indicates that the minimal O_{II}-O_{II} and Ti-Ti vertical distances are constrained to the corresponding distances in $SrTiO_3$. The nine-unit-cell-thick film exhibited a larger unit cell and larger displacements than the four-unit-cell-thick film. The four-unit-cell-thick film is one of the thinnest monodomain perovskite films observed to be in the polar phase.

The nine-unit-cell-thick film measured at 181 °C exhibits a 180° stripe domain structure. COBRA analysis was consistent with Pb and Ti atoms having two folded positions separated by about 0.4 ± 0.1 Å, depending on position in the film. The unit cell size is smaller than in the monodomain films.

The fact that the slowly cooled samples are monodomain and polarized in a unique way relative to the substrate suggests that the substrate plays an important role in the ferroelectric behavior. Studies of thicker $PbTiO_3$ films on $SrTiO_3$ substrates[24,36] have found that the polarity can be either up or down, suggesting that the sign may depend on film thickness. For ultrathin films, such as those studied here, there may be a stronger preference for up polarization. Also in these monodomain samples, we see unusual positions of the O_I atoms near the substrate interface, indicating a potential mechanism for screening of the depolarizing field. These measurements of atomic displacements, in the substrate region and throughout the film, provide the quantitative foundation needed for *ab initio* calculations of the charge distribution that stabilizes the monodomain ferroelectric phase.

In conclusion, thin ferroelectric films grown epitaxially on paraelectric substrates display a rich variety of structures and properties. The COBRA method has proven itself to be a very powerful tool in obtaining sub-Ångstrom resolution images of such films which reveal details of the film structure. We believe that this technique can be advantageously used to investigate a variety of such systems, providing the structural information necessary to elucidate the mechanisms controlling their structure and properties.

ACKNOWLEDGMENTS

The authors gratefully acknowledge experimental assistance from the APS Sectors 7, 12, and 20 beamline staff. Work supported by the U.S. Department of Energy, Basic Energy Sciences, under Contract No. W-31-109-ENG-38, and the State of Illinois. This project is supported in part by the US-Israel Bi-National Science Foundation under Contract No. 1999-187 and by DOE Grant No. DE-FG02-03ER46023.

*Electronic address: fong@anl.gov

[1] J. F. Scott, *Ferroelectric Memories* (Springer, Berlin, 2000).
[2] P. Muralt, J. Micromech. Microeng. **10**, 136 (2000).
[3] T. M. Shaw, S. Trolier-McKinstry, and P. C. McIntyre, Annu. Rev. Mater. Sci. **30**, 263 (2000).
[4] C. H. Ahn, K. M. Rabe, and J.-M. Triscone, Science **303**, 488 (2004).
[5] R. Kretschmer and K. Binder, Phys. Rev. B **20**, 1065 (1979).
[6] R. Ramesh and D. G. Schlom, Science **296**, 1975 (2002).
[7] Ph. Ghosez and K. M. Rabe, Appl. Phys. Lett. **76**, 2767 (2000).
[8] B. Meyer and D. Vanderbilt, Phys. Rev. B **63**, 205426 (2001).
[9] I. P. Batra, P. Wurfel, and B. D. Silverman, Phys. Rev. B **8**, 3257 (1973).
[10] P. Wurfel and I. P. Batra, Ferroelectrics **12**, 55 (1976).
[11] C. T. Black and J. J. Welser, IEEE Trans. Electron Devices **46**, 776 (1999).
[12] J. Junquera and Ph. Ghosez, Nature (London) **422**, 506 (2003).
[13] T. Mitsui and J. Furuichi, Phys. Rev. **90**, 193 (1953).
[14] A. M. Bratkovsky and A. P. Levanyuk, Phys. Rev. Lett. **84**, 3177 (2000).
[15] M. G. Stachiotti, Appl. Phys. Lett. **84**, 251 (2004).
[16] S. K. Streiffer, J. A. Eastman, D. D. Fong, Carol Thompson, A. Munkholm, M. V. Ramana Murty, O. Auciello, G.-R. Bai, and G. B. Stephenson, Phys. Rev. Lett. **89**, 067601 (2002).
[17] D. D. Fong, G. B. Stephenson, S. K. Streiffer, J. A. Eastman, O. Auciello, P. H. Fuoss, and Carol Thompson, Science **304**, 1650 (2004).
[18] M. Sowwan, Y. Yacoby, J. Pitney, R. MacHarrie, M. Hong, J. Cross, D. A. Walko, R. Clarke, R. Pindak, and E. A. Stern, Phys. Rev. B **66**, 205311 (2002).
[19] Y. Yacoby, M. Sowwan, E. A. Stern, J. O. Cross, D. Brewe, R. Pindak, J. Pitney, E. B. Dufresne, and R. Clarke, Nat. Mater. **1**, 99 (2001).
[20] D. K. Saldin, V. L. Shneerson, and R. Fung, Physica B **336**, 16 (2003).
[21] I. K. Robinson and J. Miao, MRS Bull. **29**, 177 (2004).
[22] N. A. Pertsev, A. G. Zembilgotov, and A. K. Tagantsev, Phys. Rev. Lett. **80**, 1988 (1998).
[23] M. J. Haun, E. Furman, S. J. Jang, H. A. McKinstry, and L. E. Cross, J. Appl. Phys. **62**, 3331 (1987).
[24] Carol Thompson, C. M. Foster, J. A. Eastman, and G. B. Stephenson, Appl. Phys. Lett. **71**, 3516 (1997).
[25] B. Meyer and D. Vanderbilt, Phys. Rev. B **65**, 104111 (2002).
[26] A. G. Zembilgotov, N. A. Pertsev, H. Kohlstedt, and R. Waser, J. Appl. Phys. **91**, 2247 (2002).
[27] A. Munkholm, S. K. Streiffer, M. V. Ramana Murty, J. A. Eastman, Carol Thompson, O. Auciello, L. Thompson, J. F. Moore, and G. B. Stephenson, Phys. Rev. Lett. **88**, 016101 (2002).
[28] M. V. Ramana Murty, S. K. Streiffer, G. B. Stephenson, J. A. Eastman, G.-R. Bai, A. Munkholm, O. Auciello, and Carol Thompson, Appl. Phys. Lett. **80**, 1809 (2002).
[29] G. B. Stephenson, J. A. Eastman, O. Auciello, A. Munkholm, Carol Thompson, P. H. Fuoss, P. Fini, S. P. DenBaars, and J. S. Speck, MRS Bull. **24** (1), 21 (1999).
[30] G. Koster, B. L. Kropman, G. J. H. M. Rijnders, D. H. A. Blank, and H. Rogalla, Appl. Phys. Lett. **73**, 2920 (1998).
[31] G. B. Stephenson, D. D. Fong, M. V. Ramana Murty, S. K. Streiffer, J. Eastman, O. Auciello, P. H. Fuoss, A. Munkholm, M. E. M. Aanerud, and Carol Thompson, Physica B **336**, 81 (2003).
[32] E. Vlieg, J. Appl. Crystallogr. **30**, 532 (1997).
[33] B. L. Henke, E. M. Gullikson, and J. C. Davis, At. Data Nucl. Data Tables **54**, 181 (1993).
[34] A. M. Glazer and S. A. Mabud, Acta Crystallogr., Sect. B: Struct. Crystallogr. Cryst. Chem. **34**, 1065 (1978).
[35] W. Zhong, R. D. King-Smith, and D. Vanderbilt, Phys. Rev. Lett. **72**, 3618 (1994).
[36] M. J. Bedzyk, A. Kazimirov, D. L. Marasco, T.-L. Lee, C. M. Foster, G.-R. Bai, P. F. Lyman, and D. T. Keane, Phys. Rev. B **61**, R7873 (2000).